Volume 49
Number 9
7 March 2020
Pages 2749-3028

Dalton Transactions

An international journal of inorganic chemistry

rsc.li/dalton

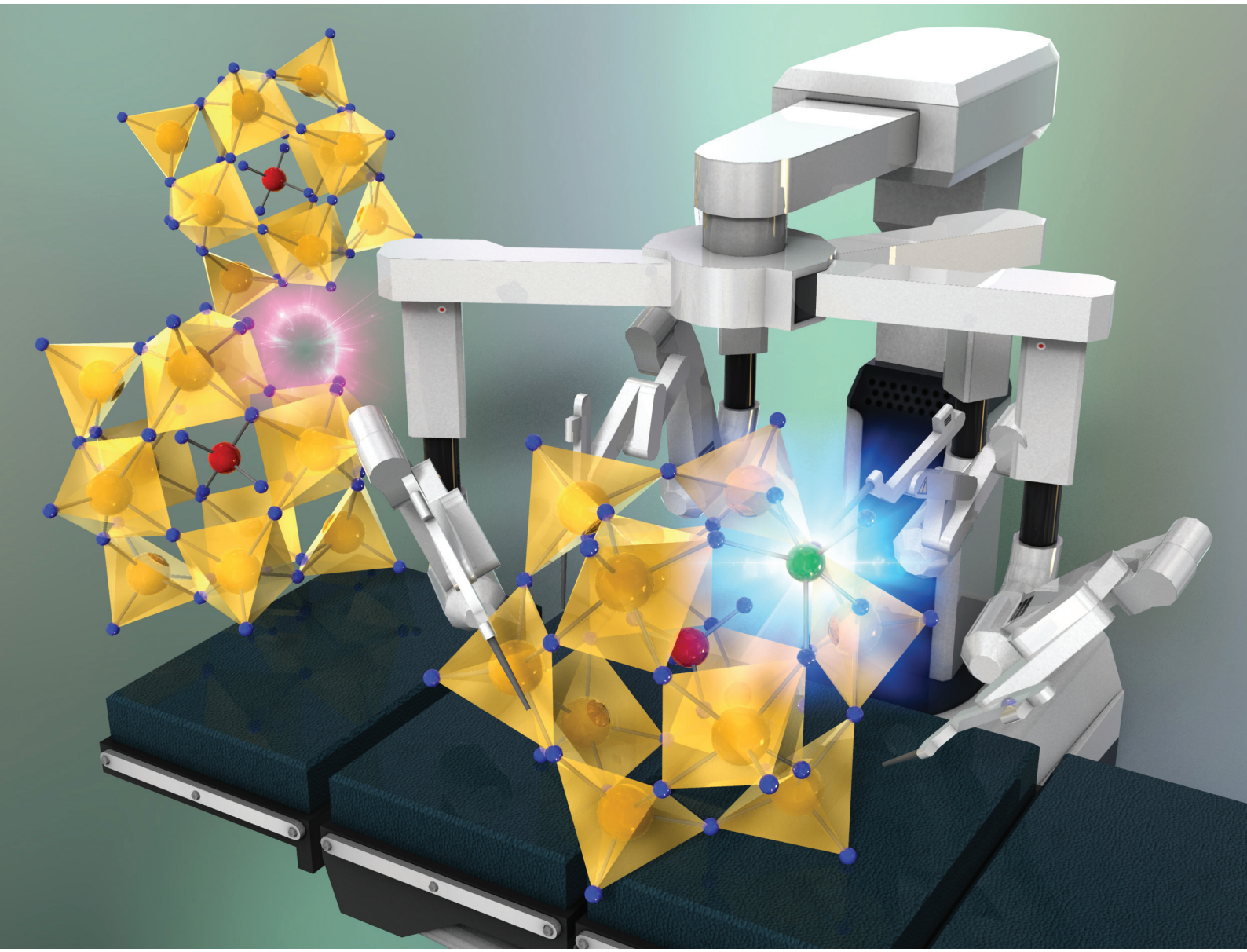

ISSN 1477-9226

ROYAL SOCIETY OF CHEMISTRY

COMMUNICATION

Tadaharu Ueda *et al.*

Metal-substituted tungstosulfates with Keggin structure: synthesis and characterization

Dalton Transactions

ROYAL SOCIETY OF CHEMISTRY

COMMUNICATION

View Article Online
View Journal | View Issue

Cite this: *Dalton Trans.*, 2020, **49**, 2766

Received 13th December 2019,
Accepted 3rd February 2020

DOI: 10.1039/c9dt04737a

rsc.li/dalton

Metal-substituted tungstosulfates with Keggin structure: synthesis and characterization†

Shinya Azuma,[a] Taiga Kadoguchi,[a] Yohei Eguchi,[a] Hikaru Hirabaru,[a] Hiromi Ota,[b] Masahiro Sadakane,[c] Kazumichi Yanagisawa,[d] Takuya Hasegawa[e] and Tadaharu Ueda *[a,f,g]

Simple synthetic procedures for accessing novel metal-substituted tungstosulfates $[SMW_{11}O_{39}]^{4-}$ with Keggin-type structures were developed based on the reaction of metal ions (M = Mn^{2+}, Co^{2+}, Ni^{2+}, and Cu^{2+}) with lacunary tungstosulfate, $[SW_{11}O_{39}]^{6-}$, which was obtained by treating $[SW_{12}O_{40}]^{2-}$ with a weak base in acetone. All metal-substituted tungstosulfates were characterized by elemental analysis, X-ray crystallography, ESI-MS, IR, Raman, UV-Vis and cyclic voltammetry analyses.

Polyoxometalates (POMs), especially Keggin-type $[XM_{12}O_{40}]^{n-}$ (X = Si, P, S, *etc.*; M = Mo and W) species, have been widely used in various fields, such as catalysts, materials chemistry, analytical chemistry and biochemistry, for both fundamental and practical applications.[1] Interestingly, Keggin-type saturated POMs, $[XM_{12}O_{40}]^{n-}$, are quite similar in size even when various heteroions with different charges are incorporated. Their redox potentials under neutral conditions, where no protonation occurs, change as a direct result of the charge of the anion or bond length of μ_4O–X: $[XW_{12}O_{40}]^{n-}$ (X = H_2, Zn, Co, B, Al, Ga, Si, Ge, P, As, and S); $[X'Mo_{12}O_{40}]^{n-}$ (X′ = Ga, Si, Ge, P, As, and S).[2] In addition, the acid strength of protonated Keggin POMs is related to the heteroatoms and addenda atoms. The acid strengths of protonated Keggin-type POMs are in the following order: $H_3PW_{12}O_{40}$ > $H_4SiW_{12}O_{40}$ > $H_3PMo_{12}O_{40}$ > $H_4SiMo_{12}O_{40}$.[3] Recently, the protonated tungstosulfate, $H_4S_2W_{18}O_{62}$, has been prepared using a new modified version of the classical etherate method, and the resulting compound exhibited better catalytic activity than $H_3PW_{12}O_{40}$ and $H_4SiW_{12}O_{40}$ for several organic reactions.[4] The sulfur-containing POMs exhibited better catalytic activities than the corresponding POMs containing other heteroatoms.

The chemical properties of POMs can change drastically upon substitution of the tungsten and molybdenum moieties in the framework with other metals.[1] The structures of the metal-incorporated (or -substituted) POMs can change, ranging from the parent Keggin- and Wells–Dawson-type structures to larger POMs, *e.g.*, sandwich-type POMs, $[M_4(XW_9O_{34})_2]^{n-}$ and $[M_4(X_2W_{15}O_{54})_2]^{n-}$ (M = transition metals). These compounds exhibit fascinating chemical properties. Cobalt- and ruthenium-bearing POMs are excellent catalysts for water oxidation. Vanadium-substituted Keggin-type POMs have been used as oxidation catalysts for a variety of organic reactions.[3,5] In addition, the redox couples of trivanadium-substituted tungstophosphate, $[PV_3W_9O_{40}]^{6-}$, make it a suitable electron carrier for redox flow batteries.[6] The redox potentials of vanadium-substituted Keggin-type and Wells–Dawson-type POMs observed under neutral conditions are related to the charge of the anion, and their potentials are similar to those of the parent (unsubstituted) Keggin-type and Wells–Dawson-type POMs, respectively: $[XVM_{11}O_{40}]^{n-}$ (X = S > As, P > Ge, Si; M = Mo and W); $[X_2VW_{17}O_{62}]^{n-}$ (X = S > As, P) and sulfur-centered Keggin-type POMs can be reduced at the most positive potential.[7] Most likely, metal-substituted tungstosulfates, $[SM'W_{11}O_{39}]^{n-}$ (M′ = transition metal), could undergo reversible redox processes at more positive potentials than the corresponding metal-substituted tungstophosphates and tungstosilicates,[8] indicating that they exhibit better cata-

[a]*Department of Applied Science, Faculty of Science, Kochi University, Kochi, 780-8520, Japan. E-mail: chuji@kochi-u.ac.jp*
[b]*Division of Instrumental Analysis, Department of Instrumental Analysis and Cryogenics, Advanced Science Research Center, Okayama University, Okayama, 700-8530, Japan*
[c]*Department of Applied Chemistry, Faculty of Engineering, Hiroshima University, Hiroshima, Japan*
[d]*Hydrothermal Reaction Center, Faculty of Science, Kochi University, Japan*
[e]*Institute of Multidisciplinary Research for Advanced Materials (IMRAM), Tohoku University, Sendai, Miyagi, 980-8577, Japan*
[f]*Department of Marine Resources, Faculty of Agriculture and Marine Science, Kochi University, Nankoku, 783-8502, Japan*
[g]*Center for Advanced Marine Core Research, Kochi University, Nankoku, 783-8520, Japan*

†Electronic supplementary information (ESI) available: Synthetic procedures, X-ray crystallography data, ionic formula, molar mass, ESI-MS spectra and IR spectra of $[SW_{11}O_{39}]^{6-}$ and $[SMW_{11}O_{39}]^{4-}$ (M = Mn^{2+}, Co^{2+}, Ni^{2+}, and Cu^{2+}) (PDF). Crystallographic data for $[SW_{11}O_{39}]^{6-}$ and $[SMW_{11}O_{39}]^{4-}$ (M = Mn^{2+}, Co^{2+}, Ni^{2+}, and Cu^{2+}) (CIF). CCDC 1968360, 1968361, 1968484, 1968486 and 1968488. For ESI and crystallographic data in CIF or other electronic format see DOI: 10.1039/C9DT04737A

lytic properties. In addition, when different types of POMs with different heteroatoms are prepared, characterized and compared with each other, many of their chemical properties can be elucidated from both experimental and theoretical perspectives. Moreover, many ambiguous chemical properties of POMs can be clarified, and their scope of applications can be broadened. However, there have been no reports on the synthesis of lacunary tungstosulfates, such as $[SW_{11}O_{39}]^{6-}$ and $[SW_9O_{34}]^{8-}$, or metal-substituted tungstosulfates, except for vanadium-substituted tungstosulfates.[9] Generally, metal-incorporated POMs can be prepared by treating the corresponding metal ions with so-called lacunary POMs, which have defects in their POM framework.[1] Recently, systematic synthetic procedures for preparing tetra-alkyl ammonium salts of Wells–Dawson-type metal-substituted tungstosulfates, $[S_2MW_{17}O_{61}]^{6-}$ (M = Mn, Co, Ni, and Cu), have been developed based on the reaction of ring-shaped $[(S_2W_{14}O_{54})_3]^{32-}$ with defects in the framework, and this starting material was prepared by treating $[S_2W_{18}O_{62}]^{4-}$ with the corresponding metal ions in a weak base.[10] All of the prepared novel POMs were characterized by X-ray crystallography, elemental analysis, ESI-MS, IR, Raman, UV-Vis and cyclic voltammetry.

In the present study, we tried to find a synthetic procedure for lacunary tungstosulfate, $[SW_{11}O_{39}]^{6-}$, which is a key compound for preparing metal-substituted tungstosulfates. In addition, systematic synthetic procedures for accessing metal-substituted tungstosulfates, $[SMW_{11}O_{39}]^{4-}$ (M = Mn^{2+}, Co^{2+}, Ni^{2+} and Cu^{2+}), were also explored and optimized. Isolated metal-substituted tungstosulfates and lacunary tungstosulfate were characterized by elemental analysis, X-ray crystallography, ESI-MS, IR, Raman, UV-Vis and cyclic voltammetry.

X-ray crystallography indicated that all novel POMs prepared in the present study had Keggin-type structures (Fig. 1; Table S1†). The mean bond lengths of SMW_{11}, SW_{11} and SW_{12} are compared in Table 1. The S–O bonds of SW_{11} and SW_{12} (1.41–1.42 Å) are shorter than that of SMW_{11} (1.49–1.51 Å). The mean bond length between tungsten and the terminal oxygens of SW_{12} (1.66 Å) is also shorter than those of SW_{11} and SMW_{11} (1.70–1.76 Å), while the other bonds are similar in length. SMW_{11} is slightly larger than SW_{12}.

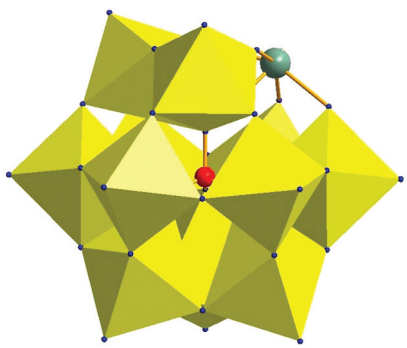

Fig. 1 Ball and stick representation of the structure of $[SMW_{11}O_{39}]^{4-}$ (M = Ni, Co, Cu, and Mn).

Table 1 Selected mean bond lengths (Å) in $[SW_{11}O_{39}]^{6-}$, $[SMW_{11}O_{39}]^{4-}$ and $[SW_{12}O_{40}]^{2-}$

POMs	S–O_a	W(M)–O_d	W(M)–O_c	W(M)–O_b	W(M)–O_a
SW_{11}	1.42	1.70	1.91	1.91	2.57
$SMnW_{11}$	1.49	1.76	1.93	1.93	2.57
$SNiW_{11}$	1.51	1.71	1.92	1.92	2.55
$SCoW_{11}$	1.50	1.70	1.91	1.91	2.54
$SMnW_{11}$	1.51	1.73	1.92	1.92	2.54
SW_{12} [a]	1.43	1.66	1.90	1.89	2.57

O_a: oxygen bound to a heteroatom; O_b: octahedral corner-sharing oxygen; O_c: octahedral edge-sharing oxygen; O_d: terminal oxygen. [a] See ref. 9.

The ESI-MS spectra of the POMs were acquired in CH_3CN to confirm the composition of the POMs (Fig. S1–S5†). The signals observed for SMW_{11} are listed in Table S2† with the corresponding calculated ionic weights per anionic charge. The signals correspond to the protonated $[SW_{11}O_{38}]^{4-}$ species rather than $[SW_{11}O_{39}]^{6-}$; this is probably because $[H_3SW_{11}O_{39}]^{3-}$ would not be stable in CH_3CN under the application of high voltage required for ion-spray ESI-MS to form $[HSW_{11}O_{38}]^{3-}$, in which one oxygen has been removed from $[H_3SW_{11}O_{39}]^{3-}$ in the form of H_2O. The simulated ESI-MS signals for the protonated forms of all metal-substituted tungstosulfates were in complete agreement with the experimental data. In the case of $SCuW_{11}$, the simulated ESI-MS signals at m/z = 914.0547, assigned to $[SCu(III)W_{11}O_{39}]^{3-}$, showed a better fit with the observed data than $[HSCu(II)W_{11}O_{39}]^{3-}$. This was due to the unexpected oxidation upon exposure to high voltage in ESI apparatus.[11] However, $SCuW_{11}$ must be $[SCu(II)W_{11}O_{39}]^{4-}$ based on the results of elemental analysis, and the ESI signals at m/z = 685.5414 can be assigned to $[SCu(II)W_{11}O_{39}]^{4-}$.

Compared to the single peak at 1167 cm^{-1} for SW_{12}, the typical IR bands at 1200–1120 cm^{-1} from the S–O bonds were split into two or three peaks for SW_{11} and SMW_{11} due to the lower symmetry around sulfur from apparent T_d to C_{3v} symmetries due to defects in the tungsten moiety and the incorporation of other metals into the framework (Fig. S6†; Table 2). Raman spectra were also acquired (Fig. S7†), and the typical Raman bands due to the symmetric stretching mode of the bond between tungsten and the terminal oxygen are listed in Table 2. The Raman band for the parent SW_{12} species appeared at 1018 cm^{-1}, while it typically appeared at approximately 980–990 cm^{-1}. By removing the tungsten unit or incorporating metal ions smaller than tungsten, the mean bond lengths (1.70–1.76 Å) of W–O_d in SW_{11} and SMW_{11} were longer than those (1.66 Å) in SW_{12}, which resulted in a shift in the Raman band to lower wavenumbers from SW_{12} to SW_{11} and SMW_{11}. For the same reason, the ligand-to-metal charge transfer (LMCT) ($O^{2-} \rightarrow W^{6+}$) bands of SW_{11} and SMW_{11} were observed at lower wavelengths than that of SW_{12} (Fig. S8†).[12]

The cyclic voltammograms of SW_{11}, SMW_{11} and SW_{12} were measured in CH_3CN containing 0.1 M n-Bu_4NPF_6 (Fig. 2). All observed waves were diffusion-controlled except for the oxi-

Table 2 Vibrational frequencies (cm^{-1}) of $[SW_{11}O_{39}]^{6-}$, $[SMW_{11}O_{39}]^{4-}$ and $[SW_{12}O_{40}]^{2-}$ in the solid state

	IR				Raman
POMs	ν(S–O_a)	ν(W–O_d)	ν(W–O_b)	ν(W–O_c)	ν(W–O_d)
SW_{12}	1167	1000	897	818	1018[a]
SW_{11}	1197	977	894	825	990
	1138		875		
	1120				
$SMnW_{11}$	1171	971	888	821	980
	1139				
$SCoW_{11}$	1196	970	886	829	982
	1167				
	1144				
$SNiW_{11}$	1152	970	888	819	982
$SCuW_{11}$	1191	971	884	820	984
	1153				

O_a: oxygen bound to a heteroatom; O_b: octahedral corner-sharing oxygen; O_c: octahedral edge-sharing oxygen; O_d: terminal oxygen. [a] See ref. 9.

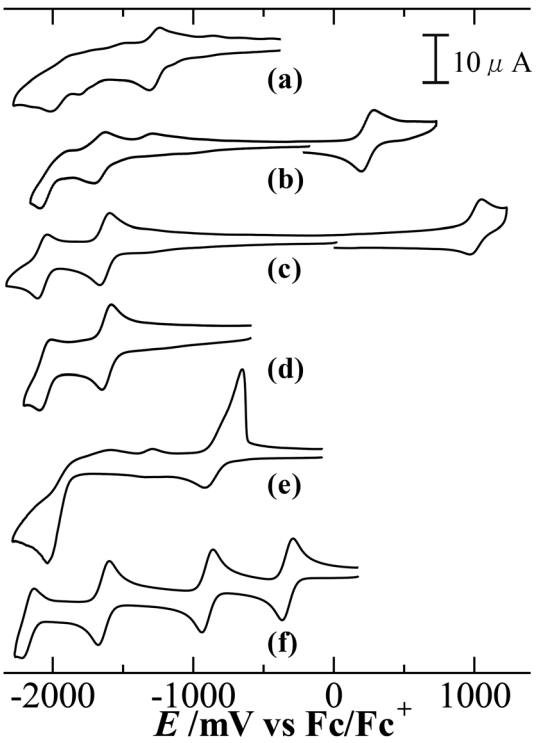

Fig. 2 Cyclic voltammograms of 0.5 mM (a) $[SW_{11}O_{39}]^{6-}$, (b) $[SMnW_{11}O_{39}]^{4-}$, (c) $[SCoW_{11}O_{39}]^{4-}$, (d) $[SNiW_{11}O_{39}]^{4-}$ and (e) $[SCuW_{11}O_{39}]^{4-}$ in CH_3CN containing 0.1 M n-Bu_4NPF_6 and (f) $[SW_{12}O_{40}]^{2-}$ in acetone containing 0.1 M n-Bu_4NPF_6. Scan rate: 100 mV s^{-1}.

dation wave that appeared at −660 mV for $SCuW_{11}$, which can be regarded as the desorption wave of copper due to a similar wave found in the voltammogram of $[PCuW_{11}O_{39}]^{5-}$.[8] The midpoint potentials for all of the observed redox waves are listed in Table 3. A quasi-reversible wave was observed at −1280 mV for SW_{11}. The one-electron reduced species would be unstable

Table 3 Midpoint potentials (mV *vs.* Fc/Fc^+) of $[SW_{11}O_{39}]^{6-}$, $[SMW_{11}O_{39}]^{4-}$ and $[SW_{12}O_{40}]^{2-}$ in CH_3CN containing 0.1 M n-Bu_4NPF_6

	Potentials (mV)			
POMs	M	W(0/1)	W(1/2)	W(2/3)
SW_{12}	—	−335	−900	−1640
SW_{11}	—	−1280		
$SMnW_{11}$	240	−1665		
$SCoW_{11}$	1000	−1630	−2075	
$SNiW_{11}$	—	−1620	−2050	
$SCuW_{11}$	−920[a], −660[b]	−2040[a]		

M represents the redox process of the incorporated metals in the POMs, and the number in parentheses indicates the number of tungsten atoms reduced from +VI to +V. [a] Reduction potential. [b] Oxidation potential.

because the following waves were irreversible. In the cases of $SMnW_{11}$ and $SCoW_{11}$, quasi-reversible redox waves were observed at 240 and 1000 mV, respectively. Coulomb number analysis by bulk electrolysis at 300 mV for $SMnW_{11}$ and 1050 mV for $SCoW_{11}$ indicated a one-electron transfer process, which revealed the oxidation of Mn(II/III) and Co(II/III), respectively. Similar oxidation waves were obtained for $[XM(H_2O)W_{11}O_{39}]^{5-}$ (X = Si, P; M = Mn, Co; XMW_{11}) in an aqueous solution or in CH_3CN.[13] Although an oxidation wave due to Mn(III/IV) was also observed for $SiMnW_{11}$, the corresponding oxidation wave was not in the range of the potential window for $SMnW_{11}$. On the other hand, the oxidation of Co(II/III) in $SCoW_{11}$ occurs at a significantly more positive potential than that of Co(II/III) in $PCoW_{11}$. Compared with the redox potential of $[\{Ru_4O_4(OH)_2(H_2O)_4\}(\gamma\text{-}SiW_{10}O_{36})_2]^{10-}$, which is a typical water oxidation POM catalyst, the $SCoW_{11}$ species could have great potential as a highly active catalyst for water oxidation; however, a simple direct comparison is not possible because different conditions were used.[14] In the case of $SCuW_{11}$, desorptive oxidation probably from Cu(0) to Cu(II) was observed at −660 mV, which is similar to what has been seen in other copper-substituted POMs after reduction of Cu(II/0) and/or Cu(I/0) in the potential range from −900 to −2100 mV.[15] However, the details of the redox mechanism of the copper component in copper-substituted POMs have not been fully elucidated. In the case of $SNiW_{11}$, no specific reduction and/or oxidation waves such as those seen in SMW_{11} (M = Mn, Co, and Cu) were observed, and only two reduction waves due to the reduction of W(VI/V) at two sites in the POM were observed in the potential window range, which is similar to what has been seen for other nickel-substituted POMs.[16] The overall voltammetric behavior of SMW_{11} is similar to that of the corresponding XMW_{11} (X = Si and P), is strongly dependent on the substituted metal (M) and is completely different from that of the parent SW_{12} species. Generally, the reduction potentials of POMs under neutral conditions, where no proton coupling reaction occurs, greatly depend on the heteroatoms or the total charge on the POMs. The order of reduction potentials is X = S > As, P > Ge, Si in Keggin-type $[XM_{12}O_{40}]^{n-}$ and $[XVM_{11}O_{40}]^{n-}$ (M = W and Mo) and in Wells–Dawson-type $[X_2M_{18}O_{62}]^{n-}$ and

$[X_2VW_{17}O_{62}]^{n-}$, and this order is almost equal to that of the acidity of the protonated forms of the POMs, *e.g.*, $H_nXM_{12}O_{40}$.[3a,17] Novel SMW_{11} species could provide access to other compounds that may be more effective catalysts than XMW_{11}(X = P, Si) in specific reactions. The details of the voltammetric behavior of $SCuW_{11}$, $SMnW_{11}$ and $SCoW_{11}$ are now being investigated, and the results will be reported in due course.

In the present study, systematic synthetic procedures for accessing $[SMW_{11}O_{39}]^{4-}$ (M = Mn^{2+}, Co^{2+}, Ni^{2+} and Cu^{2+}) were developed based on the reaction of the corresponding metal ions (M^{2+}) with lacunary $[SW_{11}O_{39}]^{6-}$, which was prepared by treating $[SW_{12}O_{40}]^{2-}$ with a weak base in acetone. The isolated tetrabutyl-ammonium salts of SMW_{11} and SW_{11} were confirmed to have Keggin-type structures by elemental analysis, X-ray crystallography and ESI-MS. In addition, all synthesized compounds were characterized by IR, Raman and UV-Vis spectroscopy and cyclic voltammetry. They exhibited spectroscopic properties similar to those of the corresponding metal-substituted tungstophosphates. In the case of SMW_{11} (M = Mn and Co), the quasi-reversible one-electron transfer redox waves corresponding to the oxidation of Mn(II/III) and Co(II/III), respectively, were observed at positive potentials. $SCuW_{11}$ gave stripping oxidation waves like those of other copper-containing POMs. The synthetic procedures for accessing the metal-substituted tungstosulfates as well as all SMW_{11} discussed in this study could open new areas of POM research, such as the development of novel POM-based materials.

Conflicts of interest

There are no conflicts to declare.

Acknowledgements

This work was supported by a Grant-in-aid for Scientific Research (No. 25410095) from the Ministry of Education, Culture, Sports, Science and Technology of Japan, a Kochi University President's Discretionary Grant, a Special Grant for Rare Metals and Green Technology, the JSPS Core-to-Core Program, and the Centre for Functional Nano Oxide at Hiroshima University. ^{183}W NMR and EPR spectra were measured at the Instrument Centre at the Institute for Molecular Science, which we would like to thank for their assistance with the measurements and for the financial support for travel and accommodations. We thank Ms. T. Amimoto at the Natural Science Centre for Basic Research and Development (N-BARD) at Hiroshima University for the ESI-MS measurements.

Notes and references

1 (*a*) M. T. Pope, *Heteropoly and Isopoly Oxometalates*, Springer, Berlin, 1983; (*b*) *Polyoxometalate Chemistry From Topology via Self-Assembly to Applications*, ed. M. T. Pope and A. Müller, Kluwer Academic Publishers, 2001; (*c*) *Polyoxometalate Chemistry for Nano-Composite Design*, ed. T. Yamase and M. T. Pope, Kluwer Academic/Plenum Publishers, 2002; (*d*) *Polyoxometalate Molecular Science*, ed. J. J. Borrás-Almenar, E. Coronado, A. Müller and M. T. Pope, Kluwer Academic Publishers, 2003; (*e*) *Polyoxometalate Chemistry – Some Recent Trends*, ed. F. Secheresse, World Scientific, 2013; (*f*) *Polyoxometalates: Properties, Structure and Synthesis*, ed. A. P. Robert, NOVA Publishers, 2016; (*g*) Polyoxometalate Chemistry, in *Advances in Inorganic Chemistry*, ed. R. V. Eldik and L. Cronin, Academic Press, Elsevier, 2017, vol. 69.

2 (*a*) K. Nakajima, K. Eda and S. Himeno, *Inorg. Chem.*, 2010, **49**, 5212–5215; (*b*) S. Himeno, M. Takamoto, R. Santo and A. Ichimura, *Bull. Chem. Soc. Jpn.*, 2005, **78**, 95–100; (*c*) K. Maeda, H. Katano, T. Osakai, S. Himeno and A. Saito, *J. Electroanal. Chem.*, 1995, **389**, 167–173.

3 (*a*) I. V. Kozhevnikov, *Chem. Rev.*, 1998, **98**, 171–198; (*b*) N. Mizuno and M. Misono, *Chem. Rev.*, 1998, **98**, 199–217.

4 T. Ueda, K. Yamashita and A. Onda, *Appl. Catal., A*, 2014, **485**, 181–187.

5 (*a*) N. Mizuno and K. Kamata, *Coord. Chem. Rev.*, 2011, **255**, 2358–2370; (*b*) O. A. Kholdeeva, N. V. Maksimchuk and G. M. Maksimov, *Catal. Today*, 2010, **157**, 107–113; (*c*) T. Ueda and H. Kotsuki, *Heterocycles*, 2008, **76**, 73–97; (*d*) M. Carraro, A. Sartorel, G. Scorrano, T. Carofiglio and M. Bonchio, *Synthesis*, 2008, 1971–1978; (*e*) C. L. Hill, *J. Mol. Catal. A: Chem.*, 2007, **262**, 2–242; (*f*) R. Neumann and A. M. Khenkin, *Chem. Commun.*, 2006, 2529–2538; (*g*) N. Mizuno and K. Yamaguchi, *Chem. Rec.*, 2006, **6**, 12–22.

6 T. Ueda, Vanadium-containing polyoxometalates: Synthesis, structure and properties, in *Polyoxometalates: Properties, Structure and Synthesis*, 2016, pp. 1–34.

7 (*a*) T. Ueda, M. Ohnishi, D. Kawamoto, S. X. Guo, J. F. Boas and A. M. Bond, *Dalton Trans.*, 2015, **44**, 11660–11668; (*b*) T. Ueda, J. Nambu, J. Lu, S. X. Guo, Q. Li, J. F. Boas, L. L. Martin and A. M. Bond, *Dalton Trans.*, 2014, **43**, 5462–5473.

8 T. Ueda, *ChemElectroChem*, 2018, **5**, 823–838.

9 S. Himeno, M. Takamoto, M. Hoshiba, A. Higuchi and M. Hashimoto, *Bull. Chem. Soc. Jpn.*, 2004, **77**, 519–524.

10 H. Hirabaru, D. Kawamoto, M. Ohnishi, H. Ota, M. Sadakane, K. Yanagisawa, T. Hasegawa and T. Ueda, *Eur. J. Inorg. Chem.*, DOI: 10.1002/ejic.201901298.

11 (*a*) G. J. Van Berkel, S. A. McLuckey and G. L. Glish, *Anal. Chem.*, 1992, **64**, 1586–1593; (*b*) G. J. Van Berkel and F. Zhou, *Anal. Chem.*, 1995, **67**, 2916–2923.

12 L. Dermeche, N. Salhi, S. Hocine, R. Thouvenot and C. Rabia, *J. Mol. Catal. A: Chem.*, 2012, **356**, 29–35.

13 (*a*) M. Sadakane and E. Steckhan, *J. Mol. Catal. A: Chem*, 1996, **114**, 221–228; (*b*) M. S. Balulla, I. A. Gamelas, H. M. Carapuça, A. M. Cavaleiro and W. Schlindwein, *Eur. J. Inorg. Chem.*, 2004, 619–628; (*c*) O. A. Kholdeeva,

M. P. Vanina, M. N. Timofeeva, R. I. Maksimovskaya, T. A. Trubitsina, M. S. Melgunov, E. B. Burgina, J. Mrowiec-Bialon, A. B. Jarzebski and C. L. Hill, *J. Catal.*, 2004, **226**, 363–371.

14 Y. Liu, S.-X. Guo, A. M. Bond, J. Zhang, Y. V. Geletii and C. L. Hill, *Inorg. Chem.*, 2013, **52**, 11986–11996.

15 B. Keita, E. Abdeljalil, L. Nadjo, B. Avisse, R. Contant, J. Canny and M. Richet, *Electrochem. Commun.*, 2000, **2**, 145–149.

16 F. A. R. S. Couto, A. M. V. Cavaleiro, J. D. Pedrosa de Jesus and J. E. J. Simão, *Inorg. Chim. Acta*, 1998, **281**, 225–228.

17 T. Ueda, K. Yamashita and A. Onda, *Appl. Catal., A*, 2014, **485**, 181–187.